Dynamics of biomembranes with active multiple-state inclusions

Hsuan-Yi Chen[1,2] and Alexander S. Mikhailov[3]
[1]*Department of Physics and Institute of Biophysics, National Central University, Jhongli 32001, Taiwan*
[2]*Institute of Physics, Academia Sinica, Taipei 11529, Taiwan*
[3]*Abteilung Physikalische Chemie, Fritz-Haber-Institut der Max-Planck-Gesellschaft, Faradayweg 4-6, 14195 Berlin, Germany*
(Received 4 July 2009; revised manuscript received 26 December 2009; published 1 March 2010)

Nonequilibrium dynamics of biomembranes with active multiple-state inclusions is considered. The inclusions represent protein molecules which perform cyclic internal conformational motions driven by the energy brought with adenosine triphosphate (ATP) ligands. As protein conformations cyclically change, this induces hydrodynamical flows and also directly affects the local curvature of a membrane. On the other hand, variations in the local curvature of the membrane modify the transition rates between conformational states in a protein, leading to a feedback in the considered system. Moreover, active inclusions can move diffusively through the membrane so that their surface concentration varies. The kinetic description of this system is constructed and the stability of the uniform stationary state is analytically investigated. We show that, as the rate of supply of chemical energy is increased above a certain threshold, this uniform state becomes unstable and stationary or traveling waves spontaneously develop in the system. Such waves are accompanied by periodic spatial variations of the membrane curvature and the inclusion density. For typical parameter values, their characteristic wavelengths are of the order of hundreds of nanometers. For traveling waves, the characteristic frequency is of the order of a thousand Hz or less. The predicted instabilities are possible only if at least three internal inclusion states are present.

DOI: 10.1103/PhysRevE.81.031901 PACS number(s): 87.16.D−, 47.54.Fj, 05.70.Np

I. INTRODUCTION

Membranes play a fundamental role in various functions of living cells, providing spatial compartmentalization and being essential for signal transduction and inter- or intracellular transport [1]. While *in vivo* experiments with biomembranes are difficult because of their strong coupling to the cytoskeleton and the cytoplasm, investigations with synthetic membranes and vesicles formed by lipid bilayers can be performed [2]. Equilibrium morphology transitions in vesicles are well described by the elastic membrane theory [3]. However, it becomes increasingly clear that, under standard physiological conditions in a living cell, biomembranes are far from the state of thermal equilibrium.

Lipid bilayers that constitute a biomembrane are usually including a large number of protein molecules which may represent ion pumps, enzymes or other molecular machines. The common property of active protein inclusions is that they undergo cyclic conformational changes, with each next cycle initiated by binding of an energy-bringing ligand, typically an adenosine triphosphate (ATP) molecule. Active conformational motions in the inclusions are coupled to the membrane dynamics, thus bringing a membrane away from the state of thermodynamic equilibrium.

Theoretical investigations of biomembranes including active ion pumps have shown [4,5] that their fluctuational power spectra must be very different from that of the equilibrium membrane systems. It has been experimentally demonstrated that active ion pumps renormalize bending rigidity [6,7] and surface tension [8] of biological membranes. In several theoretical studies, it has been furthermore predicted [9–11] that instabilities of membrane shapes may be induced by the nonequilibrium activity of the inclusions. Besides ion pumps, biomembranes containing other types active proteins have also been studied. For example, it has been shown in [12] that for membrane-membrane adhesion due to adhesive receptors, or stickers, that are actively switched between "on" and "off" states, there is a resonance switching rates at which the membrane separations are large. For membranes interacting with cytoskeleton, Shlomovitz and Gov [13] have predicted the possibility of active membrane waves driven by actin and myosin [14]. Furthermore, active fission-fusion processes encountered in intracellular trafficking may also affect the stability of a flat biomembrane [15].

The original theoretical analysis of active membrane instabilities has been performed [9] in the framework of a general phenomenological approach where the details of operation of individual protein inclusions did not play a role. Effects of conformational transitions in active protein inclusions have been explicitly considered in previous publications [10,11] where the equations for membrane dynamics have been complemented by a kinetic equation for conformational transitions in molecular inclusions. Only inclusions with two different conformational states have been previously studied.

However, models with two-state active inclusions are special and some important effects cannot be described by such kinds of models. Generally, a system out of thermal equilibrium is characterized by circulating probability flows whose existence is characteristic for the violation of the detailed balance. If only two states are present, the circulating flows are not however possible. In this sense, two-state systems are always similar to the systems at thermal equilibrium. When a two-state system is brought out of thermal equilibrium, it can still be described by some effective temperature.

Having this in mind, we construct here a complete kinetic description for the membranes with multiple-state inclusions, representing a generalization of the previous theories [4,6,10]. For the general case of the K-state inclusions, a

detailed stability analysis is analytically performed. In addition to the long-wavelength static instability due to the negative effective surface tension, two new instabilities are found. They are the Turing-type static instability with a finite spatial wavelength and the oscillatory wave-type instability with a finite wavelength. The characteristic wavelengths of both instabilities are of the order of hundreds of nanometers; the characteristic frequency of the patterns emerging as a result of the wave instability is up to a thousand Hz. Such Turing and wave instabilities are not possible if only the inclusions with two internal states are present.

Below in Sec. II the theoretical model is formulated. First the expressions for the free energy of the system are given and then the dynamical evolution equations are constructed. In Sec. III, the slow-time limit of the model, valid when the time scales of intramolecular processes are much shorter than the time scales of the merging membrane patterns, is introduced and discussed. The stability analysis of the uniform stationary state is performed in Sec. IV. The results are finally discussed in Sec. V.

II. MODEL

A. Free energy and the equilibrium state

We consider a membrane composed of lipids and active inclusions with K internal states. In this study, we assume that all inclusions have the same orientation with respect to the membrane. The situation where inclusions with both up and down orientations are present can be considered in a similar way. Before discussing the dynamics, we first consider the free energy of this system. At the coarse-grained level, its free energy is given by the sum of the elastic energy of a lipid bilayer, the free energy associated with the inclusions, and the energy of coupling between the inclusions and the membrane,

$$F = F_{mem} + F_{inc} + F_{coup}. \tag{1}$$

For a quasiflat membrane, the elastic free energy of a lipid bilayer is

$$F_{mem} = \frac{1}{2}\int d^2\mathbf{r}[\gamma(\nabla h)^2 + \kappa(\nabla^2 h)^2 + k_2(\nabla^3 h)^2], \tag{2}$$

where h is the height of the membrane relative to the reference plane, $\mathbf{r}=x\hat{\mathbf{i}}+y\hat{\mathbf{j}}$ is the two-dimensional position vector in the reference plane and $\nabla=\partial_x\hat{\mathbf{i}}+\partial_y\hat{\mathbf{j}}$. The coefficient γ characterizes surface tension of the membrane, since the system under consideration is a biomimetic membrane, we take the surface tension of typical cell membranes as the upper limit for the magnitude of γ, i.e, $\gamma \lesssim 5\times 10^{-3} k_B T/\mathrm{nm}^2$ [16]. κ specifies the bending rigidity of the membrane, typically $\kappa \sim 10 k_B T$ [17]. The coefficient k_2 characterizes membrane rigidity with respect to the spatial variation of the curvature. Typically, $k_2 \sim a^2\kappa \sim 300 k_B T\cdot \mathrm{nm}^2$ ($a\sim 5$ nm is the linear size of an inclusion), this term is negligible on lengths large compared to an inclusion. However, as we will show, for membranes containing active multiple-state inclusions, it is possible that the active forces in the system result in an effective negative membrane bending rigidity. Only when this type of instabilities occurs, k_2 term becomes essential and determines the instability wavelength. Otherwise, this term will be neglected.

The free energy associated with the inclusions is

$$F_{inc} = n_0\int d^2r\left\{k_B T\left[\sum_\alpha \phi_\alpha \ln\phi_\alpha + \left(1-\sum_\alpha \phi_\alpha\right)\times\ln\left(1-\sum_\alpha \phi_\alpha\right)\right] + \sum_\alpha E_\alpha\phi_\alpha\right\}, \tag{3}$$

where $0\le\phi_\alpha\le 1$ is the dimensionless surface density of inclusions in the state $\alpha(\alpha=1,2,3,\ldots,K)$, E_α is the energy of an inclusion in the state α, $n_0=1/a^2$. In this paper, we consider the case of low inclusion density and neglect therefore possible direct lateral interactions between the inclusions.

The coupling between the inclusion density and the local membrane curvature is

$$F_{coup} = \int d^2r\kappa\sum_\alpha c_\alpha\phi_\alpha\nabla^2 h, \tag{4}$$

where c_α are the coefficients specifying the strength of coupling between inclusions in different internal states α and the local membrane curvature. When $c_\alpha>0$, membrane regions rich in the inclusions in the state α tend to have $\nabla^2 h<0$. The coefficient c_α has the dimensionality of the inverse length, $c_\alpha\sim\Delta\Sigma_\alpha/\Sigma_\alpha l_\alpha$, where Σ_α is the average cross-sectional area, $\Delta\Sigma_\alpha$ is the difference between the outer and the inner leaflet surface area of a state-α inclusion and l_α is the thickness (in the z direction) of the inclusion (see Appendix for the explanations). Typically, c_α is of the order of $c_\alpha\lesssim 0.1\ \mathrm{nm}^{-1}$.

The equilibrium state of the system satisfies the conditions $\delta F/\delta h=0$ and $\delta F/\delta\phi_\alpha=0$. This leads to the equations determining the equilibrium state,

$$\kappa\nabla^4 h - \gamma\nabla^2 h - k_2\nabla^6 h + \kappa\sum_\alpha c_\alpha\nabla^2\phi_\alpha = 0 \tag{5}$$

and

$$\kappa c_\alpha\nabla^2 h + k_B T n_0\left[\ln\phi_\alpha - \ln\left(1-\sum_\beta\phi_\beta\right)\right] + n_0 E_\alpha = 0. \tag{6}$$

Equation (6) gives us

$$\phi_\alpha = \left(1-\sum_\beta\phi_\beta\right)\exp[-(E_\alpha + n_0^{-1}\kappa c_\alpha\nabla^2 h)/k_B T]. \tag{7}$$

Therefore, the local total density of inclusions at thermal equilibrium is

$$\phi_t = \sum_\alpha\phi_\alpha = \frac{\sum_\alpha \exp[-(E_\alpha + n_0^{-1}\kappa c_\alpha\nabla^2 h)/k_B T]}{1+\sum_\alpha \exp[-(E_\alpha + n_0^{-1}\kappa c_\alpha\nabla^2 h)/k_B T]}. \tag{8}$$

Note that the total number of inclusions present in the membrane is $N=n_0\int d^2\mathbf{r}\phi_t$. It depends on E_α, implying that E_α includes a contribution from the free-energy difference between an α-state inclusion in the membrane and an α-state inclusion in the solvent.

Because we are primarily interested in nonequilibrium behavior, we limit our study below to the situations where the

uniform flat state of the membrane is stable under equilibrium conditions.

B. Evolution equations

If a membrane is impermeable, it can only move together with the solvent flow. A (partially) permeable membrane can be dragged through the solvent. Thus, the equation for the temporal evolution of $h(\mathbf{r},t)$ is

$$\partial_t h = \mathbf{v}\cdot\hat{\mathbf{n}} - \lambda_p\left[\frac{\delta F}{\delta h} + \sum_{\alpha,\beta} k_{\alpha\beta} n_0 P^m_{\alpha\beta}\phi_\beta\right], \tag{9}$$

where $\mathbf{v}(\mathbf{r})$ is the velocity of the local solvent flow and $\hat{\mathbf{n}}(\mathbf{r})$ is the unit normal vector of the membrane surface. Because of the permeation, the solvent can "leak" from one side of the membrane to the other. If a force f is locally applied at a permeable membrane, it gets dragged through the solvent with the velocity $v=\lambda_p f$, where λ_p is the permeation constant, typically $\lambda_p \lesssim 10^{-12}$ $\mathrm{m}^3/\mathrm{N\ s}$ [18]. The local force f is given by the expression in the brackets in Eq. (9). In addition to the first contribution, directly coming from the free energy, it also includes the second term of purely kinetic origin. When an inclusion changes its internal conformational state, some force acting on the membrane is generated. Such average force corresponds to the second term inside the brackets. Here, $k_{\alpha\beta}$ is the transition rate constant for an inclusion to go from the state β to the state α. In general α and β are integers between 1 and K, but for inclusions with cyclic transitions such as ion pumps, $k_{\alpha\beta}$ is nonvanishing only for $\beta=\alpha\pm 1$. $P^m_{\alpha\beta}$ is the momentum that an inclusion delivers to the membrane during a $\beta\to\alpha$ conformational change. Typically, $P^m_{\alpha\beta}$ ranges from $\mathrm{pN}\cdot\mu\mathrm{s}$ to $\mathrm{pN}\cdot\mathrm{m\ s}$. In our analysis, we shall neglect thermal noises acting on the membrane, which should be generally present in the membrane evolution equation.

The local density of inclusions in the state α changes with time because of the lateral diffusion and the conformational transitions between the states, so that the evolution equations for the surface densities of inclusions in the state α are

$$\partial_t \phi_\alpha = M_\alpha \nabla^2 \frac{\delta F}{\delta \phi_\alpha} + \sum_\beta [k_{\alpha\beta}\phi_\beta - k_{\beta\alpha}\phi_\alpha], \tag{10}$$

where M_α is the mobility coefficient for the inclusions in the state α.

Hydrodynamic flows in the solvent are described by the modified Stokes equation in the limit of low Reynolds number that takes into account the elastic stress due to the membrane and the forces resulting from the inclusion conformational changes [6,10]. We have

$$\begin{aligned} 0 = &-\nabla p - \partial_z p\hat{\mathbf{z}} + \eta(\nabla^2+\partial_z^2)\mathbf{v} - \delta(z-h)\frac{\delta F}{\delta h}\hat{\mathbf{n}} \\ &+ \sum_{\alpha\beta} k_{\alpha\beta} n_0 P_{\alpha\beta}\phi_\beta[(1+z^{(u)}_{\alpha\beta}\nabla^2 h)\delta(z-z^{(u)}_{\alpha\beta}-h) \\ &-(1-z^{(d)}_{\alpha\beta}\nabla^2 h)\delta(z+z^{(d)}_{\alpha\beta}-h)]\hat{\mathbf{n}}, \end{aligned} \tag{11}$$

where η is the viscosity of the solvent. In this equation,

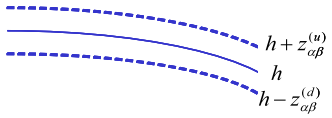

FIG. 1. (Color online) Force centers of the active force dipoles for $\beta\to\alpha$ transitions are distributed on surfaces described by $h+z^{(u)}_{\alpha\beta}$, and $h-z^{(d)}_{\alpha\beta}$. These surfaces and $h(\mathbf{r})$ are parallel surfaces, the areas of parallel surface elements from top to bottom are $(1-z^{(u)}_{\alpha\beta}\nabla^2 h)dA$, dA, and $(1+z^{(d)}_{\alpha\beta}\nabla^2 h)dA$, respectively.

$\delta F/\delta h$ corresponds to the pressure jump across the membrane due to the membrane elasticity. The last term comes from the conformational changes of the inclusions, and it is further discussed in the following: Because the dynamics of an inclusion in the fluid is strongly overdamped, an inclusion exerts a zero net force on the solvent during its conformational transition from the state β to the state α. The simplest description for the effect of an inclusion conformational change on the solvent flow is therefore provided by a model of a force dipole. Hence, $z^{(u)}_{\alpha\beta}$ and $z^{(d)}_{\alpha\beta}$ in Eq. (11) are the characteristic lengths (both on the order of a nanometer) for the force distribution, and $P_{\alpha\beta}$ is the momentum transfer to the solvent, during a conformational change of an inclusion from the state β to the state α. As has been previously pointed out in Ref. [19] (but neglected in Refs. [7,10]), because force centers of the inclusions lie in the surfaces parallel to the membrane (see Fig. 1), the local density of the force centers in the plane $h+z^{(u)}_{\alpha\beta}$ is $(1+z^{(u)}_{\alpha\beta}\nabla^2 h)\delta(z-z^{(u)}_{\alpha\beta}-h)$ and the local density of the force centers in the plane $h-z^{(d)}_{\alpha\beta}$ is $(1-z^{(d)}_{\alpha\beta}\nabla^2 h)\delta(z+z^{(d)}_{\alpha\beta}-h)$. The physical meaning and typical magnitudes of the parameters entering into Eqs. (9)–(11) are listed in Table I.

We note that in [6] $P_{\alpha\beta}$ is conveniently chosen to be equal to $P^m_{\alpha\beta}$. This describes force dipoles that are composed of the action-reaction force pairs between the inclusion and the membrane. In our model, we have chosen a more general situation where $P^m_{\alpha\beta}$ does not have to be the same as $P_{\alpha\beta}$.

In addition, because the solvent is incompressible we have

$$\nabla\cdot\mathbf{v} + \partial_z v_z = 0. \tag{12}$$

C. Microscopic reversibility and detailed balance

Microscopic reversibility imposes several constraints on $k_{\alpha\beta}$, $P^m_{\alpha\beta}$, $P_{\alpha\beta}$, $z^{(u)}_{\alpha\beta}$, and $z^{(d)}_{\alpha\beta}$. The local membrane curvature affects the energy landscape of the conformational states of an inclusion, thus in general the transition rates $k_{\alpha\beta}$ should depend on the local membrane curvature. To the order of $\nabla^2 h$ we have

$$k_{\alpha\beta} = \Omega^{(0)}_{\alpha\beta} k^{(0)}_{\alpha\beta}(1+\Omega^{(1)}_{\alpha\beta} l_{\alpha\beta}\nabla^2 h). \tag{13}$$

Here, the parameters $k^{(0)}_{\alpha\beta}$ and $l_{\alpha\beta}$ correspond to passive inclusions in the absence of external energy supply; $k^{(0)}_{\alpha\beta}$ is the equilibrium transition rate at the zero local membrane curvature and $l_{\alpha\beta}$ represents the characteristic length associated with the curvature dependence of the equilibrium transition rate. The parameters $\Omega^{(0)}_{\alpha\beta}$ and $\Omega^{(1)}_{\alpha\beta}$ are introduced to describe

TABLE I. Coefficients in Eqs. (2)–(4), (21), and (22) and their typical values.

Symbol	Physical meaning	Typical value
κ	Membrane bending modulus	$\sim 10k_BT$
γ	Membrane surface tension	$\lesssim 5\times 10^{-3}k_BT/\mathrm{nm}^2$
c_α	Inclusion-curvature coupling constant	$\lesssim 0.1\ \mathrm{nm}^{-1}$
k_2	Higher bending modulus of the membrane	$\sim 300k_BT\cdot\mathrm{nm}^2$
a	Lateral linear size of an inclusion	5 nm
n_0	$1/a^2$	$\sim 0.04\ \mathrm{nm}^{-2}$
η	Solvent viscosity	~ 0.01–$0.1\ \mathrm{g/cm\cdot s}$
$k_{\alpha\beta}$	Inclusion conformational transition rate constant	$\sim \mathrm{m\ s}^{-1}$-$\mu\mathrm{s}^{-1}$
$P^m_{\alpha\beta}$	Momentum transfer to the membrane for $\beta\to\alpha$ inclusion conformational change	$\sim \mathrm{pN}\cdot\mu\mathrm{s}$-$\mathrm{pN}\cdot\mathrm{m\ s}$
$P_{\alpha\beta}$	Momentum transfer to the solvent for $\beta\to\alpha$ inclusion conformational change	$\sim \mathrm{pN}\cdot\mu\mathrm{s}$-$\mathrm{pN}\cdot\mathrm{m\ s}$
$z^{(u)}_{\alpha\beta}$, $z^{(d)}_{\alpha\beta}$	Characteristic lengths associated with active force during $\beta\to\alpha$ transition	$\sim$nm

changes in these properties when inclusions become active, i.e., when the energy is supplied to the inclusions. Thus, for passive inclusions $\Omega^{(0)}_{\alpha\beta}=\Omega^{(1)}_{\alpha\beta}=1$ and the transition rates take the equilibrium form $k_{\alpha\beta}=k^e_{\alpha\beta}=k^{(0)}_{\alpha\beta}(1+l_{\alpha\beta}\nabla^2 h)$.

The detailed balance condition implies (to the order h) the following relationship between the equilibrium transition rates $k^e_{\alpha\beta}$ and $k^e_{\beta\alpha}$:

$$\frac{k^e_{\alpha\beta}}{k^e_{\beta\alpha}}=\frac{e^{-(E_\alpha+n_0^{-1}\kappa c_\alpha\nabla^2 h)/k_BT}}{e^{-(E_\beta+n_0^{-1}\kappa c_\beta\nabla^2 h)/k_BT}}=e^{-(E_\alpha-E_\beta)/k_BT}\left(1-\frac{\kappa(c_\alpha-c_\beta)}{n_0k_BT}\nabla^2 h\right). \tag{14}$$

The second expression is valid as long as $\kappa(c_\alpha-c_\beta)\nabla^2 h/n_0k_BT=[\kappa(c_\alpha-c_\beta)/n_0k_BT]/R\ll 1$, where $R=|\nabla^2 h|^{-1}$ is the radius of the local membrane curvature. The above condition yields

$$\frac{k^{(0)}_{\alpha\beta}}{k^{(0)}_{\beta\alpha}}=e^{-(E_\alpha-E_\beta)/k_BT}, \tag{15}$$

and

$$l_{\alpha\beta}-l_{\beta\alpha}=-\frac{\kappa(c_\alpha-c_\beta)}{n_0k_BT}. \tag{16}$$

When the system is passive, there can be no active permeation. Therefore, we have

$$\sum_{\alpha\beta}k^e_{\alpha\beta}P^m_{\alpha\beta}\phi_\beta=0. \tag{17}$$

The requirement of the detailed balance $k^e_{\alpha\beta}\phi^e_\beta=k^e_{\beta\alpha}\phi^e_\alpha$ yields

$$P^m_{\alpha\beta}=-P^m_{\beta\alpha}. \tag{18}$$

This relationship is a direct consequence of the microscopic reversibility of an $\alpha\to\beta$ transition: the momentum transfer from an inclusion to the membrane during an $\alpha\to\beta$ transition has the same magnitude but opposite direction as the momentum transfer from an inclusion to the membrane during a $\beta\to\alpha$ transition.

Two other conditions, that must be satisfied for passive systems, are

$$\begin{cases}\displaystyle\sum_{\alpha\beta}k^e_{\alpha\beta}P_{\alpha\beta}(z^{(u)}_{\alpha\beta}+z^{(d)}_{\alpha\beta})\phi_\beta=0,\\ \displaystyle\sum_{\alpha\beta}k^e_{\alpha\beta}P_{\alpha\beta}(z^{(u)2}_{\alpha\beta}-z^{(d)2}_{\alpha\beta})\phi_\beta=0.\end{cases}$$

Again, because of the detailed balance, these two conditions lead to

$$P_{\alpha\beta}=-P_{\beta\alpha}, \tag{19}$$

and

$$z^{(u)}_{\alpha\beta}=z^{(u)}_{\beta\alpha},\quad z^{(d)}_{\alpha\beta}=z^{(d)}_{\beta\alpha}. \tag{20}$$

These conditions are also direct consequences of microscopic reversibility.

When detailed balance is violated, Eqs. (16) and (18)–(20) are still valid as microscopic motions are not changed, but the transition rate $k_{\alpha\beta}$ is different from $k^e_{\alpha\beta}$. In particular, $\Omega^{(0)}_{\alpha\beta}-1$ indicates how far the system is driven away from equilibrium, $\Omega^{(1)}_{\alpha\beta}-1$ indicates how much the curvature dependence of the active transition rate differs from the equilibrium system.

D. Final evolution equations

By using Eqs. (11) and (12) and applying the Fourier transformation in the coordinate space, the flow velocity $\mathbf{v}$ can be expressed in terms of the height variation h. Substituting the resulting expressions into Eqs. (9) and (10), final evolution equations for the local membrane height and the inclusion density in different conformation states are obtained. They have the form

$$\partial_t h(\mathbf{q},t) = -\lambda_p \left[\frac{\delta F}{\delta h} + \sum_{\alpha\beta} k_{\alpha\beta} n_0 P^m_{\alpha\beta} \phi_\beta \right](\mathbf{q},t) - \frac{1}{4\eta q} \left[\frac{\delta F}{\delta h} + \sum_{\alpha\beta} k_{\alpha\beta} n_0 P_{\alpha\beta} \phi_\beta (z^{(u)}_{\alpha\beta} + z^{(d)}_{\alpha\beta}) q^2 h + \sum_{\alpha\beta} k_{\alpha\beta} n_0 P_{\alpha\beta} \frac{z^{(u)2}_{\alpha\beta} - z^{(d)2}_{\alpha\beta}}{2} q^2 \phi_\beta \right](\mathbf{q},t), \tag{21}$$

and

$$\partial_t \phi_\alpha(\mathbf{q},t) = -M_\alpha q^2 \frac{\delta F}{\delta \phi_\alpha}(\mathbf{q},t) + \sum_\beta (k_{\alpha\beta}\phi_\beta - k_{\beta\alpha}\phi_\alpha)(\mathbf{q},t). \tag{22}$$

Here $h(\mathbf{q},t)$ and $\phi_\alpha(\mathbf{q},t)$ are the coefficients of the Fourier expansion of the local height $h(\mathbf{r},t)$ and the local densities $\phi_\alpha(\mathbf{r},t)$ over the plane waves $\exp(i\mathbf{q}\cdot\mathbf{r})$.

The contributions to the membrane dynamics given by Eq. (21) come (i) from the elastic stress of the membrane, described by $\delta F/\delta h$, (ii) from the direct momentum transfer from the inclusions to the lipid bilayer, described by $k_{\alpha\beta} n_0 P^m_{\alpha\beta} \phi_\beta$, (iii) from the action of the active force dipoles due to the coupling between the local membrane curvature and the force density distribution, described by $k_{\alpha\beta} n_0 P_{\alpha\beta} \phi_\beta (z^{(u)}_{\alpha\beta} + z^{(d)}_{\alpha\beta}) q^2 h$, and (iv) from the action of the active force quadrupoles due to the up-down asymmetry of the shape of the inclusions [19], described by $k_{\alpha\beta} n_0 P_{\alpha\beta} (z^{(u)2}_{\alpha\beta} - z^{(d)2}_{\alpha\beta}) q^2 \phi_\beta / 2$.

Evolution Eqs. (21) and (22) provide the final concise description of the membrane dynamics coupled to the kinetic transitions in active multiple-state inclusions diffusing within the membrane. The physical meanings and typical magnitudes of the parameters entering into these equations and the respective expressions for the free energy are summarized in Table I.

Equations (21) and (22) represent the generalization of the equations previously obtained in the studies [5,9,19] where conformational changes inside the inclusions were neglected, while the active momentum transfer from the inclusions to the membrane [5,9] and the active force dipoles and active force quadrupoles [19] were taken into account.

III. LIMIT OF SLOW MEMBRANE DYNAMICS

Membrane motions with long wavelengths are slow. The characteristic time scales of such motions are much larger than the characteristic times corresponding to the kinetics of internal transitions inside the inclusions. In this situation, which we consider further in our study, the steady nonequilibrium distribution over the internal states of active inclusions should be adiabatically following the changes in the local membrane shape.

As an example, we can consider biomembranes with active ion pumps, such as bacteriorhodopsin (BR) and Ca^{2+}-ATPase, which have been used in the experiments [6–8]. The typical timescale for conformational transitions inside the cycle in these ion pumps is of the order of several milliseconds. The lateral diffusion constant for an ion pump inside a membrane is of the order of 1 $\mu m^2/s$. Therefore, within a single active conformational cycle such an inclusion would move over the distance of about several tens of nanometers inside the membrane. Hence, if the membrane shape varies on a scale of several hundreds of nanometers or longer, the adiabatical approximation for the inclusion kinetics shall be applicable.

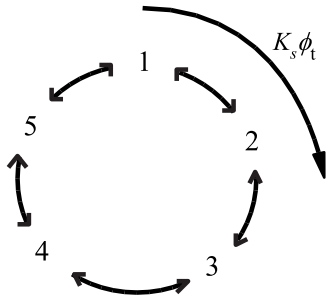

FIG. 2. Schematics of conformational transitions of an inclusion with five internal states.

In the steady state, local inclusion densities satisfy equations

$$\sum_\beta (k_{\alpha\beta}\phi_\beta - k_{\beta\alpha}\phi_\alpha) = 0 \quad \text{for all} \quad \alpha. \tag{23}$$

In this paper, inclusions with cyclic transitions are considered (Fig. 2) so that $k_{\alpha\beta}=0$ for $\beta-\alpha \neq \pm 1$. Therefore, Eq. (23) gives us

$$k_{21}\phi_1 - k_{12}\phi_2 = k_{32}\phi_2 - k_{23}\phi_3 = k_{43}\phi_3 - k_{34}\phi_4 = \cdots \equiv K_s(k_{\alpha\beta})\phi_t. \tag{24}$$

Thus, conformational transitions are characterized by a steady conformational current $K_s\phi_t$. When $K_s>0$ the conformational current is along $1\to 2\to 3\to \ldots \to K\to 1$. The presence of such a flow (if K_s is not vanishing) indicates the absence of the detailed balance and a deviation from the state of thermal equilibrium for the inclusions. It is also clear from Eqs. (23) and (24) that for inclusions with only two states, the conformational current always vanishes.

Slow dynamics of the system is described by two variables: the membrane height h and the overall local density of inclusions $\phi_t=\Sigma_\alpha \phi_\alpha$. From Eq. (22), we obtain

$$\partial_t \phi_t(\mathbf{r},t) = \sum_\alpha M_\alpha \nabla^2 \left(k_B T n_0 \ln \frac{\phi_\alpha}{1-\phi_t} + \kappa c_\alpha \nabla^2 h \right). \tag{25}$$

Here, ϕ_α depends on ϕ_t and K_s, we will discuss this dependence when deriving the linearized equations. To find the equation for h, the terms related to active forces are simplified by introducing the active momentum transfer, the active force dipole and the active force quadrupole associated with an inclusion. From Eqs. (18), (19), and (24), we obtain

$$\sum_{\alpha\beta} k_{\alpha\beta} P^m_{\alpha\beta} \phi_\beta = (P^m_{21} + P^m_{32} + \cdots + P^m_{KK-1} + P^m_{1K})(k_{21}\phi_1 - k_{12}\phi_2) \equiv P^m_A K_s(k_{\alpha\beta})\phi_t, \tag{26}$$

$$\sum_{\alpha\beta} k_{\alpha\beta}P_{\alpha\beta}(z^{(u)}_{\alpha\beta}+z^{(d)}_{\alpha\beta})\phi_\beta=[P_{21}(z^{(u)}_{21}+z^{(d)}_{21})+P_{32}(z^{(u)}_{32}+z^{(d)}_{32}) + \cdots + P_{1K}(z^{(u)}_{1K}+z^{(d)}_{1K})](k_{21}\phi_1 - k_{12}\phi_2) \equiv p_A K_s \phi_t. \quad (27)$$

and

$$\sum_{\alpha\beta} k_{\alpha\beta}P_{\alpha\beta}\frac{z^{(u)2}_{\alpha\beta}-z^{(d)2}_{\alpha\beta}}{2}\phi_\beta=\left(P_{21}\frac{z^{(u)2}_{21}-z^{(d)2}_{21}}{2}+P_{32}\frac{z^{(u)2}_{32}-z^{(d)2}_{32}}{2} + \cdots + P_{1K}\frac{z^{(u)2}_{1K}-z^{(d)2}_{1K}}{2}\right)(k_{21}\phi_1 - k_{12}\phi_2) \equiv Q_A K_s \phi_t. \quad (28)$$

Here, we have defined the active momentum transfer from an inclusion to the membrane during one cycle $P^m_A=P^m_{21}+P^m_{32}+\cdots+P^m_{1K}$, the net active force dipole of an inclusion during one cycle $p_A=P_{21}(z^{(u)}_{21}+z^{(d)}_{21})+P_{32}(z^{(u)}_{32}+z^{(d)}_{32})+\cdots+P_{1K}(z^{(u)}_{1K}+z^{(d)}_{1K})$ and the net active force quadrupole of an inclusion during one cycle $Q_A=P_{21}(z^{(u)2}_{21}-z^{(d)2}_{21})/2+P_{32}(z^{(u)2}_{32}-z^{(d)2}_{32})/2+\cdots+P_{1K}(z^{(u)2}_{1K}-z^{(d)2}_{1K})/2$. Note that the respective terms are nonvanishing and thus contribute to the membrane dynamics only when the detailed balance is violated and the cyclic conformational current $K_s\phi_t$ is present. The equation of motion for $h(\mathbf{q},t)$ can be obtained by substituting Eq. (26)–(28) into Eq. (21), yielding

$$\partial_t h(\mathbf{q},t) = -\lambda_p\left[\frac{\delta F}{\delta h}+n_0P^m_A K_s\phi_t\right](\mathbf{q},t)-\frac{1}{4\eta q}\left[\frac{\delta F}{\delta h}+n_0 p_A K_s\phi_t h q^2+n_0 Q_A K_s\phi_t q^2\right](\mathbf{q},t). \quad (29)$$

Equation (29) indicates that the membrane acquires a nonzero velocity due to active permeation, as one can see from $\partial_t h=-\lambda_p n_0 P^m_A K_s\phi_t$ at $q=0$. For a permeable membrane this drift provides clear manifestation of nonequilibrium processes in the system under consideration. However, so far the experiments on active membranes have been carried out only for the membranes with negligible permeability and the active drift could not be observed [6].

IV. NONEQUILIBRIUM INSTABILITIES

To analyze possible instabilities of the flat membrane, we should linearize the equations of motion by expanding $h(\mathbf{r},t)$ and $\phi_t(\mathbf{r},t)$ around their uniform solutions $h_0(t)$ and ϕ_{t0},

$$h(\mathbf{r},t)=h_0(t)+\delta h(\mathbf{r},t),$$

$$\phi_t(\mathbf{r},t)=\phi_{t0}+\delta\phi_t(\mathbf{r},t). \quad (30)$$

Note that $\delta h(\mathbf{q},t)=h(\mathbf{q},t)$ and $\delta\phi_t(\mathbf{q},t)=\phi_t(\mathbf{q},t)$ for $q\neq 0$.

First, we consider the linear elasticity of the system. One can express $\delta F/\delta h$ as

$$\frac{\delta F}{\delta h(\mathbf{r})}=(\kappa\nabla^4-\gamma\nabla^2-k_2\nabla^6)h+\sum_\alpha \kappa c_\alpha\nabla^2\left(\frac{\phi_\alpha}{\phi_t}\phi_t\right).$$

At small $\nabla^2 h$, we can further express ϕ_α/ϕ_t as

$$\frac{\phi_\alpha}{\phi_t}=\psi_\alpha(1+l_{\psi\alpha}\nabla^2 h+\cdots), \quad (31)$$

where ψ_α is dimensionless and $l_{\psi\alpha}$ is a length that characterizes the curvature dependence of ϕ_α/ϕ_t. Because all coordinate dependence of ϕ_α/ϕ_t comes from the local curvature dependence of the transition rates, both ψ_α and $l_{\psi\alpha}$ are independent of $\mathbf{r}$, but they depend on $\Omega^{(0)}_{\alpha\beta}$ and $\Omega^{(1)}_{\alpha\beta}$, i.e., on the strength of the external energy drive. From Eq. (31), $\nabla^2(\phi_t\phi_\alpha/\phi_t)=\psi_\alpha\nabla^2\phi_t+\psi_\alpha l_{\psi\alpha}\phi_{t0}\nabla^4 h+\cdots$. As a result,

$$\frac{\delta F}{\delta h(\mathbf{r})}=\kappa\left(1+\sum_\alpha c_\alpha\psi_\alpha l_{\psi\alpha}\phi_{t0}\right)\nabla^4 h-\gamma\nabla^2 h-k_2\nabla^6 h + \sum_\alpha \kappa c_\alpha\psi_\alpha\nabla^2\phi_t=\kappa_{eff}\nabla^4 h-\gamma\nabla^4 h-k_2\nabla^6 h + \kappa_{eff}c^h_{eff}\nabla^2\phi_t. \quad (32)$$

Here, we have introduced the effective membrane bending rigidity $\kappa_{eff}=\kappa(1+\Sigma_\alpha c_\alpha\psi_\alpha l_{\psi\alpha}\phi_{t0})$ and the effective inclusion-membrane elastic coupling constant $c^h_{eff}=\Sigma_\alpha c_\alpha\psi_\alpha\kappa/\kappa_{eff}$. Note that, besides of c_α, the coefficients κ_{eff} and c^h_{eff} also depend on $\Omega^{(0)}_{\alpha\beta}$ and $\Omega^{(1)}_{\alpha\beta}$ through ψ_α and $l_{\psi\alpha}$. These effective elastic moduli are different from their equilibrium values because the relative inclusion population ϕ_α/ϕ_t is different from the equilibrium distribution.

Next we consider the equation for $\delta\phi_t$. From Eq. (31),

$$\nabla^2\left(\ln\frac{\phi_\alpha}{1-\phi_t}\right)=\nabla^2\left(\ln\frac{\phi_\alpha}{\phi_t}+\ln\frac{\phi_t}{1-\phi_t}\right) = l_{\psi\alpha}\nabla^4 h+\left(\frac{1}{\phi_{t0}}+\frac{1}{1-\phi_{t0}}\right)\nabla^2\delta\phi_t.$$

Substituting the above expression into Eq. (25), one finds

$$\partial_t\delta\phi_t=\sum_\alpha M_\alpha\left\{n_0k_BT\left[l_{\psi\alpha}\nabla^4 h+\left(\frac{1}{\phi_{t0}}+\frac{1}{1-\phi_{t0}}\right)\nabla^2\delta\phi_t\right]+\kappa c_\alpha\nabla^4 h\right\}.$$

It is convenient to introduce the effective mobility $M_{eff}\equiv\Sigma_\alpha M_\alpha$, the effective susceptibility of the inclusions $\chi_{eff}\equiv n_0k_BT[1/\phi_{t0}+1/(1-\phi_{t0})]$ and the effective inclusion-membrane elastic coupling constant c^ϕ_{eff} associated with inclusion diffusion, $M_{eff}\kappa_{eff}c^\phi_{eff}\equiv\Sigma_\alpha M_\alpha(\kappa c_\alpha+n_0k_BTl_{\psi\alpha})$. Similar to κ_{eff} and c^h_{eff}, c^ϕ_{eff} depends on $\Omega^{(0)}_{\alpha\beta}$ and $\Omega^{(1)}_{\alpha\beta}$. Now the equation for $\partial_t\phi_t(\mathbf{q},t)$ can be written as

$$\partial_t\phi_t(\mathbf{q},t)=-M_{eff}(\chi_{eff}q^2\phi_t(\mathbf{q},t)-\kappa_{eff}c^\phi_{eff}q^4 h(\mathbf{q},t)). \quad (33)$$

To obtain the linearized equation for $\partial h(\mathbf{q},t)/\partial t$, we expand the conformational current to the order of h as $K_s(k_{\alpha\beta})=K_0(1+l_K\nabla^2 h+\cdots)$ and obtain

$$K_s(k_{\alpha\beta})\phi_t=K_0\phi_{t0}+K_0\delta\phi_t+K_0l_K\phi_{t0}\nabla^2 h, \quad (34)$$

where K_0 and l_K are both independent of $\mathbf{r}$, but they depend on $\Omega^{(0)}_{\alpha\beta}$ and $\Omega^{(1)}_{\alpha\beta}$. Substituting Eqs. (32) and (34) into Eq.

TABLE II. Coefficients in Eq. (40).

Symbols	Definition	Physical meaning
ψ_α, $l_{\psi\alpha}$	$\phi_\alpha/\phi_t=\psi_\alpha(1+l_{\psi\alpha}\nabla^2 h)$	ϕ_α/ϕ_t represents the distribution over the internal state α
κ_{eff}	$\kappa(1+\Sigma_\alpha\psi_\alpha l_{\psi\alpha}\phi_{t0})$	Effective bending rigidity in $\delta F/\delta h$
c^h_{eff}	$\Sigma_\alpha c_\alpha\psi_\alpha\kappa/\kappa_{eff}$	Inclusion-curvature coupling in $\delta F/\delta h$
c^ϕ_{eff}	$\Sigma_\alpha M_\alpha(\kappa c_\alpha+n_0k_BTl_{\phi\alpha})/M_{eff}\kappa_{eff}$	Inclusion-curvature coupling in $\partial\phi_t/\partial t$
K_0	$K_s=K_0(1+l_K\nabla^2 h)$	$K_0\phi_t$ is the curvature-independent conformational current
l_K	$K_s=K_0(1+l_K\nabla^2 h)$	$K_0l_k(\nabla^2 h)\phi_{t0}$ is the curvature-dependent conformational current
γ_a	$\gamma+n_0p_AK_0\phi_{t0}$	Surface tension renormalized by the active force dipoles
κ_a	$\kappa_{eff}-n_0Q_AK_0l_K\phi_{t0}$	Bending rigidity renormalized by the curvature-induced active quadrupoles
c_a	$(\kappa_{eff}c^h_{eff}-n_0Q_AK_0)/\kappa_{eff}$	Inclusions-curvature coupling renormalized by the curvature-independent active force quadrupoles

(29), a linearized equation of motion for $h(\mathbf{q},t)$ in the momentum space is found,

$$\partial_t h(\mathbf{q},t)=-\lambda_p[(\gamma^p_a q^2+\kappa_{eff}q^4+k_2q^6)h(\mathbf{q},t)-(\kappa_{eff}c^h_{eff}q^2-n_0P^m_AK_0)\phi_t(\mathbf{q},t)\}-\frac{1}{4\eta q}[(\gamma_a q^2+\kappa_a q^4+k_2q^6)h(\mathbf{q},t)-\kappa_{eff}c_aq^2\phi_t(\mathbf{q},t)]. \quad (35)$$

In this equation, the following notations have been introduced:

$$\gamma^p_a=\gamma-n_0P^m_AK_0l_K\phi_{t0} \quad (36)$$

is the surface tension renormalized by the active forces with which the inclusions act on the membrane,

$$\gamma_a=\gamma+n_0p_AK_0\phi_{t0} \quad (37)$$

is the surface tension renormalized by the active force dipoles,

$$\kappa_a=\kappa_{eff}-n_0Q_AK_0l_K\phi_{t0} \quad (38)$$

is the bending rigidity renormalized by the curvature-induced active quadrupoles, and

$$\kappa_{eff}c_a=\kappa_{eff}c^h_{eff}-n_0Q_AK_0 \quad (39)$$

defines the renormalized inclusion-curvature coupling due to the curvature-independent active force quadrupoles.

Since experiments are usually carried out for the membranes with negligible permeability [6–8], we consider below only the instabilities of impermeable membranes with $\lambda_p=0$.

It is convenient to write the derived equations in the matrix form

$$\partial_t\begin{pmatrix}h(\mathbf{q},t)\\ \phi_t(\mathbf{q},t)\end{pmatrix}=\begin{pmatrix}M_{hh}(q) & M_{h\phi}(q)\\ M_{\phi h}(q) & M_{\phi\phi}(q)\end{pmatrix}\begin{pmatrix}h(\mathbf{q},t)\\ \phi_t(\mathbf{q},t)\end{pmatrix}, \quad (40)$$

where

$$M_{hh}(q)=-\frac{q}{4\eta}(\gamma_a+\kappa_aq^2+k_2q^4),$$

$$M_{h\phi}(q)=\frac{q}{4\eta}\kappa_{eff}c_a,$$

$$M_{\phi h}(q)=M_{eff}\kappa_{eff}c^\phi_{eff}q^4,$$

$$M_{\phi\phi}(q)=-M_{eff}\chi_{eff}q^2. \quad (41)$$

The definitions and physical meanings of the parameters in Eqs. (40) and (41) are summarized in Table II.

To analyze the linear stability of the system, we seek solutions of Eq. (40) of the form $h(\mathbf{q},t)$, $\phi_t(\mathbf{q},t)\sim e^{\lambda t}$. The characteristic equation for λ is

$$\lambda^2-(M_{hh}+M_{\phi\phi})\lambda+(M_{hh}M_{\phi\phi}-M_{\phi h}M_{h\phi})=0. \quad (42)$$

Let the two solutions of the above equation be $\lambda_1(\mathbf{q})$ and $\lambda_2(\mathbf{q})$. Then

$$\lambda_1+\lambda_2=M_{hh}+M_{\phi\phi}=-\frac{1}{4\eta}(\gamma_aq+4\eta M_{eff}\chi_{eff}q^2+\kappa_aq^3+k_2q^5),$$

$$\lambda_1\lambda_2=M_{hh}M_{\phi\phi}-M_{h\phi}M_{\phi h}=\frac{M_{eff}\chi_{efff}}{4\eta}(\gamma_aq^3+\tilde{\kappa}_aq^5+k_2q^7), \quad (43)$$

where

$$\tilde{\kappa}_a=\kappa_a-\frac{\kappa^2_{eff}c_ac^\phi_{eff}}{\chi_{eff}}. \quad (44)$$

The following instabilities can occur in this system:

(i) the long-wavelength instability at $q=0$ when one of the λ's becomes zero at $q=0$ and both λ_1, λ_2 are negative for any nonzero q;

TABLE III. Typical magnitudes of the parameters important for the stability analysis.

Symbol	Typical magnitude
p_A	$\lvert p_A\rvert/a \lesssim$ pN·m s
Q_A	$\lvert Q_A\rvert/a^2 \lesssim$ pN·m s
K_0	$\lvert K_0\rvert \lesssim$ m s
$K_0 l_K \nabla^2 h$	$\lvert K_0 l_K \nabla^2 h\rvert \lesssim$ m s
ϕ_{t0}	$\phi_{t0} \lesssim 0.1$
χ_{eff}	$\chi_{eff} \sim k_B T/\mathrm{nm}^2$
κ_{eff}	$\kappa_{eff} \lesssim 10 k_B T$
c^h_{eff}, c^ϕ_{eff}	$\lvert c^h_{eff}\rvert, \lvert c^\phi_{eff}\rvert \lesssim 0.1$ nm^{-1}

(ii) the oscillatory wave instability (a Hopf bifurcation with a finite wave number) at $q=q_h$, when $\lambda_1+\lambda_2=M_{hh}(q)+M_{\phi\phi}(q)<0$ for all q except $q=q_h$ and $\lambda_1\lambda_2=M_{hh}(q)M_{\phi\phi}(q)-M_{h\phi}(q)M_{\phi h}(q)>0$ for all q. The frequency of the wave at the onset of the instability is $\omega/2\pi=\sqrt{\lambda_1(q_h)\lambda_2(q_h)}/2\pi$.

(iii) The static Turing-type instability, when $\lambda_1+\lambda_2<0$ for all q and $\lambda_1\lambda_2>0$ for all q except $q=q_s$.

The typical magnitudes of the parameters that are important for the stability analysis are summarized in Table III. Figure 3 shows phase diagrams for systems with the typical parameters. Varying the parameters does not change qualitative features of the phase diagrams. The ordinates in Fig. 3 represent the strength of the curvature-dependent pumping and the abscissas represent the strength of the curvature-independent pumping. The state of thermal equilibrium corresponds to the origin of coordinates; as the system is driven out of equilibrium, the state of the system moves along a straight line with the slope l_K/a. Generally, coefficients κ_{eff}, c^ϕ_{eff}, and c^h_{eff} also vary as the system is being moved away of equilibrium; for simplicity we take however constant values $\kappa_{eff}=5k_BT$, and $c^\phi_{eff}=c^h_{eff}=0.1$ nm^{-1} when the phase boundaries below in Fig. 3 are determined. We have conveniently chosen the z-axis of the system such that the signs of both c^h_{eff} and c^ϕ_{eff} are positive. Thus the possible nonequilibrium phases of an active membrane depend only on the signs of p_A and Q_A.

(a) When $p_A>0$ and $Q_A>0$, an active membrane containing inclusions that has l_K/a greater than the slope of the dashed line of Fig. 3(a) has a Turing-type instability when it is driven sufficiently far away from equilibrium. Otherwise, the system has a wave instability.

(b) When $p_A>0$ and $Q_A<0$, an active membrane containing inclusions with $l_K<0$ has a Turing-type instability when it is driven sufficiently far away from equilibrium.

(c) When $p_A<0$ and $Q_A>0$, an active membrane containing inclusions that has l_K/a greater than the slope of the dashed line of Fig. 3(c) has a Turing-type instability when it is driven sufficiently far away from equilibrium. Otherwise, the system has a long-wavelength instability.

(d) When $p_A<0$ and $Q_A<0$, an active membrane containing inclusions with $\lvert l_K/a\rvert$ greater than the absolute value of the slope of the dashed line of Fig. 3(d) has a Turing-type instability when it is driven sufficiently far away from equilibrium. Otherwise, the system has a long-wavelength instability.

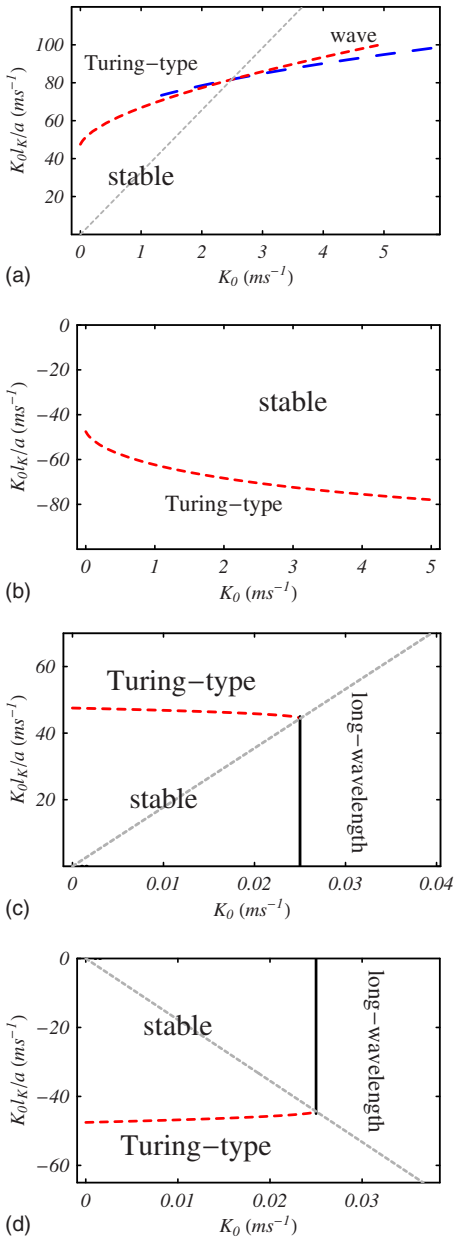

FIG. 3. (Color online) Nonequilibrium phase diagrams for the membranes with active multistate inclusions. Here $\gamma=10^{-4}k_BT/\mathrm{nm}^2$, $k_2=250k_BT\cdot\mathrm{nm}^2$, $\phi_{t0}=0.1$, $M_{eff}\chi_{eff}=1$ μm^2/s, and $\eta=10^{-3}$ kg/m·s. The long-dashed curve indicates the onset of the wave instability, the short-dashed curve indicates the onset of the Turing instability, and the solid line indicates the onset of the long-wavelength instability. (a) $p_A/a=1$ pN·m s, $Q_A/a^2=1$ pN·m s. (b) $p_A/a=1$ pN·m s, $Q_A/a^2=-1$ pN·m s. (c) $p_A/a=-1$ pN·m s, $Q_A/a^2=1$ pN·m s. (d) $p_A/a=-1$ pN·m s, $Q_A/a^2=-1$ pN·m s.

A. Long-wavelength static instability

According to Eq. (43), this instability occurs when $\gamma_a=\gamma+n_0p_AK_0\phi_{t0}<0$, i.e., when the effective surface tension

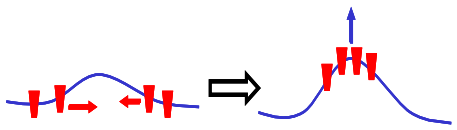

FIG. 4. (Color online) The Turing-type instability: (i) the inclusions are attracted to the regions with the preferred membrane curvature, (ii) the curvature-dependent active force quadrupoles generate membrane curvature that attracts the inclusions.

becomes negative. As shown in Fig. 3, for systems with $p_A < 0$ this instability is possible at sufficiently large K_0. Using as the typical values $|p_A| \sim \text{nm}\cdot\text{pN}\cdot\mu\text{s}$ to $\text{nm}\cdot\text{pN}\cdot\text{m s}$, $K_0 \lesssim \text{m s}^{-1}$ and $n_0 = a^{-2} \sim 1/25\ \text{nm}^2$, we find that to get $\gamma_a < 0$ for a relatively low inclusion density, such as $\phi_{t0} \lesssim 10^{-1}$, a vesicle with a bare surface tension $\gamma \lesssim 10^{-3} k_B T/\text{nm}^2$ is needed. In the experiments [8], the measured surface tension of a vesicle with passive BRs was $\gamma \sim 10^{-4} k_B T/\text{nm}^2$. Thus, it should be possible to observe this long-wavelength instability in the experiments.

B. Finite-wavelength instabilities

Besides of the long-wavelength instability corresponding to negative γ_a, there are also instabilities when κ_a or $\tilde{\kappa}_a$ become negative. If γ_a is positive, these instabilities correspond to the growth of modes with finite wavelengths, because long-wavelength fluctuations are suppressed by membrane tension.

(i) When

$$\tilde{\kappa}_a = -2\sqrt{\gamma_a k_2}, \tag{45}$$

the static Turing-type instability takes place. Its characteristic wave number is

$$q_s = (\gamma_a/k_2)^{1/4}. \tag{46}$$

As follows from Eqs. (37), (38), and (44), Eq. (45) is equivalent to

$$n_0 Q_A K_0 \left(l_K \phi_{t0} - \frac{\kappa_{eff} c^{\phi}_{eff}}{\chi_{eff}} \right) - 2\sqrt{(\gamma + n_0 p_A K_0 \phi_{t0}) k_2} = \kappa_{eff} - \frac{\kappa^2_{eff} c^{\phi}_{eff} c^{h}_{eff}}{\chi_{eff}}. \tag{47}$$

As seen in Fig. 4, two conditions are essential for the occurrence of this instability. The first is that the difference $\kappa_{eff} - \kappa^2_{eff} c^{\phi}_{eff} c^{h}_{eff}/\chi_{eff}$ should be small, implying that the curved membrane regions are strongly attracting the inclusions. The second property is that the combination $n_0 Q_A K_0 (l_K \phi_{t0} - \kappa_{eff} c^{\phi}_{eff}/\chi_{eff})$ should be large and positive, implying strong curvature-induced active force quadrupoles. In the phase diagrams in Fig. 3, the Turing-type instability is located where $K_0 l_K$ is large.

The characteristic wavelength at the onset of the Turing-type instability can be estimated. Taking $\gamma_a \sim \gamma \lesssim 5 \times 10^{-3} k_B T/\text{nm}^2$, $k_2 \sim 300 k_B T \cdot \text{nm}^2$, we find that this finite-wavelength instability has a characteristic wavelength of $2\pi/q_s = 2\pi/(\gamma_a/k_2)^{1/4} \gtrsim 10\ \text{nm} - 10^2\ \text{nm}$. Numerically computed wavelengths for this instability are shown in Fig. 5. Note also that, according to Figs. 3 and 5, for $p_A < 0$ only the membranes with inclusions that have large l_K (i.e., the conformational current of the inclusions increases rapidly with the local membrane curvature) may exhibit the Turing-type instability, otherwise long-wavelength instability is taking place.

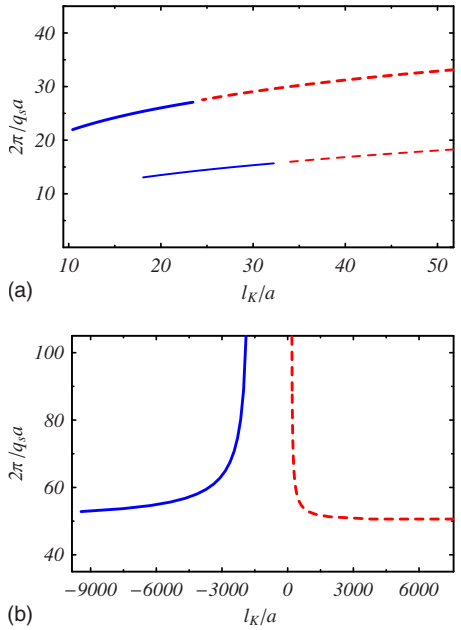

FIG. 5. (Color online) The characteristic wavelengths at the onset of instabilities plotted as functions of l_K/a, the dimensionless coefficient for the curvature-dependent pumping rate. $\gamma = 10^{-4} k_B T/\text{nm}^2$, $k_2 = 250 k_B T \cdot \text{nm}^2$, $\phi_{t0} = 0.1$, $M_{eff}\chi_{eff} = 1\ \mu\text{m}^2/\text{s}$, $\eta = 10^{-3}\ \text{kg/m}\cdot\text{s}$. $\kappa_{eff} = 5 k_B T$, and $c^{h}_{eff} = c^{\phi}_{eff} = 0.1\ \text{nm}^{-1}$. (a) thin curves: $p_A/a = 1\ \text{pN}\cdot\text{m s}$, $Q_A/a^2 = 1\ \text{pN}\cdot\text{m s}$ (dashed curve: wave instability; solid curve: Turing-type instability); thick curves: $p_A/a = 0.1\ \text{pN}\cdot\text{m s}$, $Q_A/a^2 = 1\ \text{pN}\cdot\text{m s}$ (dashed curve: wave instability, solid curve: Turing-type instability). (b) dashed curve: $p_A/a = -1\ \text{pN}\cdot\text{m s}$, $Q_A/a^2 = 1\ \text{pN}\cdot\text{m s}$; and solid curve: $p_A/a = -1\ \text{pN}\cdot\text{m s}$, $Q_A/a^2 = -1\ \text{pN}\cdot\text{m s}$.

(ii) When $\kappa_a = \kappa^c_a$, the oscillatory wave instability with the characteristic wave vector q_h takes place. The values of κ_a and q_h are given by the solutions of two equations,

$$q_h = \sqrt{\frac{-\kappa^c_a}{6k_2} + \sqrt{\left(\frac{-\kappa^c_a}{6k_2}\right)^2 + \frac{\gamma_a}{3k_2}}}, \tag{48}$$

and

$$2q^3_h + \frac{\kappa^c_a}{k_2} q_h + \frac{2\eta M_{eff}\chi_{eff}}{k_2} = 0. \tag{49}$$

Because $q_h > 0$, Eq. (48) requires κ^c_a to be negative.

Generally, the above equations for κ^c_a and q_h have to be solved numerically. Figure 3 shows that this instability may occur only when p_A, Q_A, and c^{h}_{eff}, c^{ϕ}_{eff} all have the same sign and the curvature-induced pumping is not too strong (i.e., l_K is not very large). These conditions suggest the following picture for the mechanism of wave instability. As shown in Fig. 6, inclusions are first attracted to the regions with their

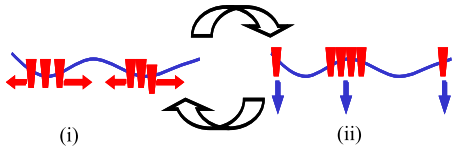

FIG. 6. (Color online) The wave instability: (i) as indicated by the horizontal arrows, inclusions are attracted to the regions with the preferred membrane curvature, this leads to (ii) as indicated by the vertical arrows, in the inclusion-rich domains, the active force quadrupoles produce the membrane curvature that repels the inclusions, therefore the system evolves back to (i).

preferred membrane curvature, but the active forces from the inclusions in these regions produce curvature that the inclusion dislike (thus l_K cannot be large). As a result, the inclusions move back and forth, chasing regions with the preferred membrane curvature. This leads to an oscillatory instability with the characteristic wavelength which is large as compared to the molecular scale. Such oscillatory instability is somewhat similar but different from the active membrane waves predicted for membranes interacting with actin and myosin [13]. Although violation of detailed balance is required for both types of waves, in the system considered in [13] conformational changes of membrane proteins and motors were neglected. Instead convex membrane proteins that activate actin polymerization, sufficiently strong myosin contraction and myosin binding to actin filaments are shown to be necessary for propagating waves in [13].

The characteristic wavelength at the onset of the wave instability in our model is about $2\pi/q_h \sim 100$ nm. Substituting q_h to $\omega_h = \sqrt{\lambda_1(q_h)\lambda_2(q_h)}$, the characteristic time period at the onset of the wave instability is estimated to be of the order of a millisecond (see Fig. 7 for numerically computed characteristic time at the onset of the wave instability). This is already on the border of the validity of the adiabatic approximation of slow membrane dynamics because such characteristic time is comparable with the time scale of conformational transitions in individual active inclusions. Therefore, our analysis of the wave instability should be

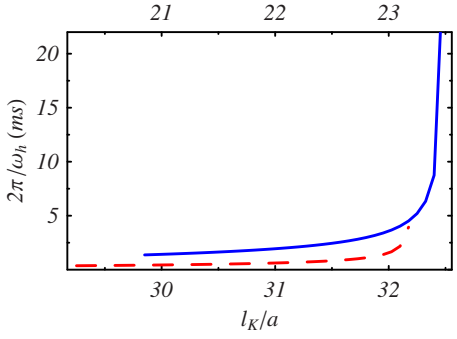

FIG. 7. (Color online) The characteristic time scales at the onset of the wave instability for $\gamma = 10^{-4} k_B T/\text{nm}^2$, $k_2 = 250 k_B T \cdot \text{nm}^2$, $\phi_{t0} = 0.1$, $M_{eff}\chi_{eff} = 1$ $\mu\text{m}^2/\text{s}$, $\eta = 10^{-3}$ kg/m·s. $\kappa_{eff} = 5 k_B T$, and $c^h_{eff} = c^{\phi}_{eff} = 0.1$ nm^{-1}. Dashed curve: $p_A/a = 1$ pN·m s, $Q_A/a^2 = 1$ pN·m s; solid curve: $p_A/a = 0.1$ pN·m s, $Q_A/a^2 = 1$ pN·m s. The magnitude of l_K/a for the solid curve is indicated at the top of the frame, and the magnitude of l_K/a for the dashed curve is indicated at the bottom.

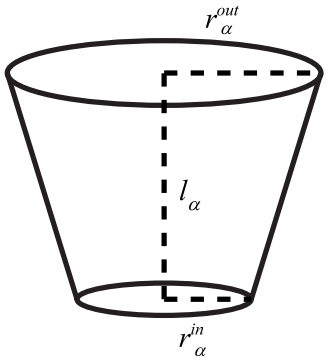

FIG. 8. A conical inclusion in state α: l_α is the thickness of the inclusion, r^{out}_α is the outer radius, and r^{in}_α is the inner radius of the inclusion.

viewed as only providing an indication that such an instability may exist. The accurate quantitative analysis of this instability should be performed without assuming the slowness of membrane dynamics; it will be undertaken in a separate publication [20].

V. DISCUSSION

We have constructed a complete kinetic description for the membranes with active multiple-state inclusions. Although we assume that all inclusions have the same orientation with respect to the membrane, the situation where inclusions with both orientations are present would be a straightforward extension of this work. Comparing to previous theories of active membranes [9,10,19], our work has several important new aspects.

First, our model includes conformational transitions for inclusions with an arbitrary number of internal states. One should note that Eqs. (21) and (22) are not a simple generalization of the previous theories. The coefficients $k_{\alpha\beta}$, $P_{\alpha\beta}$, $P^m_{\alpha\beta}$, $z^{(u)}_{\alpha\beta}$, and $z^{(d)}_{\alpha\beta}$ obey certain relations imposed by the microscopic time-reversal symmetries of the system. This is the first theoretical study where such a connection between the hydrodynamics and the microscopic dynamics of active membranes is established. An important feature of this connection is that the kinetic coefficients in our model can be extracted from the microscopic models of individual inclusions [21]. Thus, a bottom-up theoretical study of the biomembrane dynamics becomes possible.

Second, we point out that only when the inclusions have at least three internal states, deviations from the detailed balance accompanied by circulating probability currents are possible. This is clearly demonstrated by the conformational current [Eqs. (23) and (24)] in the limit of slow membrane dynamics. Nonequilibrium properties of an active membrane with two-state inclusions in previous study [10] can be attributed to the fact that the kinetic coefficients corresponding to active forcing in [10] did not obey the microscopic time-reversal symmetry. Hence, the study [10] should be rather considered as corresponding to a model for a membrane containing active multiple-state inclusions, in the limit that two of the conformations of an inclusion have much longer life-

times than all other conformations. An advantage of our present formulation is that, unlike in [10], it is now possible to obtain the conformational current $K_s\phi_t$ from the microscopic models of individual inclusions [21].

We have performed a linear stability analysis and constructed nonequilibrium phase diagrams of active membranes. We find that the type of instability depends on the signs of the force dipole and the force quadrupole of the active inclusions. The characteristic wavelengths of the Turing type and the traveling-wave instabilities are both of the order of hundreds of nanometers. The characteristic frequency of the traveling wave is of the order of a kHz. Experimentally, the static Turing instability could be observed directly by an optical microscope, and dynamic scattering experiments can be applied to probe both stationary and traveling waves.

To further study the instabilities predicted in the present analysis, numerical simulations should be performed in the future [20]. The full dynamics, including the amplitudes of the Turing type and the traveling waves, and the effect of thermal fluctuations on the instabilities, will be further examined in these simulations.

ACKNOWLEDGMENTS

One of the authors (H.Y.C.) acknowledges stimulating discussions with J-F. Joanny and P. Bassereau and is grateful for the hospitality provided during his stay at the Institute Curie in Paris. He is supported by the National Science Council of the Republic of China (Taiwan) under the Grant No. NSC 96-2628-M-008-001-MY2, and by the National Center for Theoretical Sciences. The other author (A.S.M.) acknowledges financial support of the German Science Foundation (DFG) through Programme No. SFB 555 "Complex Nonlinear Processes."

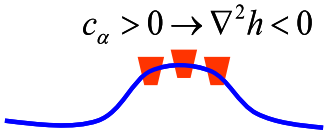

FIG. 9. (Color online) Regions rich in the inclusions with positive c_α tend to have $\nabla^2 h < 0$.

APPENDIX

In this appendix we give a brief calculation that relates the shape of a conical state-α inclusion to the coupling constant c_α.

As shown in Fig. 8, the outer radius, the inner radius and the thickness of a state-α inclusion are r_α^{out}, r_α^{in}, and l_α, respectively. The preferred radius of curvature R_α is related to these quantities by

$$\frac{r_\alpha^{out}}{R_\alpha + l_\alpha/2} = \frac{r_\alpha^{in}}{R_\alpha - l_\alpha/2}.$$

That is,

$$R_\alpha = \frac{l_\alpha (r_\alpha^{out} + r_\alpha^{in})/2}{r_\alpha^{out} - r_\alpha^{in}} = \frac{(r_\alpha^{out} + r_\alpha^{in})^2 l_\alpha/2}{(r_\alpha^{out^2} - r_\alpha^{in^2})} \sim \frac{\Sigma_\alpha l_\alpha}{\Delta\Sigma_\alpha}, \quad \text{(A1)}$$

where Σ_α is the average cross-sectional area of a state-α inclusion, $\Delta\Sigma_\alpha$ is the difference of cross-sectional area between the outer and the inner surfaces of a state-α inclusion. The coupling constant c_α is simply $c_\alpha \sim 1/R_\alpha$. As follows from Eqs. (2) and (4), the regions that are rich in the inclusions with $c_\alpha > 0$ tend to have $\nabla^2 h < 0$. This is illustrated in Fig. 9.

[1] H. Lodish *et al.*, *Molecular Cell Biology*, 3rd ed. (W.H. Freeman, New York, 1995).
[2] E. Sackmann, J. Phys.: Condens. Matter **18**, R785 (2006).
[3] U. Seifert, Adv. Phys. **46**, 13 (1997).
[4] J. Prost and R. Bruinsma, Europhys. Lett. **33**, 321 (1996).
[5] S. Sankararaman, G. I. Menon, and P. B. Sunil Kumar, Phys. Rev. E **66**, 031914 (2002).
[6] J.-B. Manneville, P. Bassereau, S. Ramaswamy, and J. Prost, Phys. Rev. E **64**, 021908 (2001).
[7] P. Girard, J. Prost, and P. Bassereau, Phys. Rev. Lett. **94**, 088102 (2005).
[8] M. D. El Alaoui Faris, D. Lacoste, J. Pècrèaux, J.-F. Joanny, J. Prost, and P. Bassereau, Phys. Rev. Lett. **102**, 038102 (2009).
[9] S. Ramaswamy, J. Toner, and J. Prost, Phys. Rev. Lett. **84**, 3494 (2000).
[10] H.-Y. Chen, Phys. Rev. Lett. **92**, 168101 (2004).
[11] C.-H. Chen and H.-Y. Chen, Phys. Rev. E **74**, 051917 (2006).
[12] B. Różycki, R. Lipowsky, and T. R. Weikl, Phys. Rev. Lett. **96**, 048101 (2006); B. Różycki, T. R. Weikl, and R. Lipowsky, Eur. Phys. J. E **22**, 97 (2007).
[13] R. Shlomovitz and N. S. Gov, Phys. Rev. Lett. **98**, 168103 (2007); Phys. Rev. E **78**, 041911 (2008).
[14] C.-H. Chen, F.-C. Tsai, C.-C. Wang, and C.-H. Lee, Phys. Rev. Lett. **103**, 238101 (2009).
[15] S. Ramaswamy and Madan Rao, C. R. Acad. Sci., Ser. IV Phys. Astrophys. **2**, 817 (2001), special issue on physics at the scale of the cell.
[16] D. Needham and R. M. Hochmuth, Biophys. J. **61**, 1664 (1992).
[17] H. Strey, M. Peterson, and E. Sackmann, Biophys. J. **69**, 478 (1995).
[18] M. Jansen and A. Blume, Biophys. J. **68**, 997 (1995); M. Jansen, Ph.D. thesis, Universität Keiserslautern, 1994; R. Lawaczeck, Biophys. J. **45**, 491 (1984); E. Boroske, M. Elwenspoek, and W. Helfrich, *ibid.* **34**, 95 (1981).
[19] M. A. Lomholt, Phys. Rev. E **73**, 061913 (2006).
[20] H.-Y. Chen and A. S. Mikhailov (unpublished).
[21] Y. Togashi and A. S. Mikhailov, Proc. Natl. Acad. Sci. U.S.A. **104**, 8697 (2007).